Experimental study of square and rectangular hollow section aluminium alloy columns

Experimental study of square and rectangular hollow section aluminium alloy columns

Shafayat Bin Ali, Evangelia Georgantzia, George S. Kamaris, Michaela Gkantou[1] and Patryk Kot

School of Civil Engineering and Built Environment, Liverpool John Moores University, Liverpool L3 3AF, United Kingdom

Abstract. Recently, aluminium alloys are extensively used in the construction sector because of their small self-weight, good corrosion resistance, low maintenance, high recyclability, and aesthetic appearance. However, one of the main disadvantages of these alloys is the low Young's modulus, which may cause a stability issue of aluminium structural members. Moreover, currently available design standards for predicting buckling resistance of aluminium columns are generally conservative. Therefore, additional research is required to evaluate the actual structural behaviour of aluminium columns under axial compression. The present study experimentally investigated the buckling response of 13 square and rectangular 6082-T6 aluminium alloy columns subjected to axial compression. The properties of the aluminium alloy were achieved from tensile test of coupon samples. The compressive load was employed concentrically by using a knife-edge hinge to ensure pin supports on both ends of the specimens. The structural response of the columns observed from the tests is presented in terms of ultimate strengths, failure modes and load-mid-height lateral displacement relationship. Furthermore, the test results of the specimens are compared with the ultimate strengths calculated by Eurocode 9, showing that the latter provides conservative and scattered design estimations.

Keywords. aluminium alloy, square hollow section (SHS), rectangular hollow section (RHS), axial compression, tubular columns, experimental study, buckling

1. Introduction

Recently, aluminium alloys have become the second most important material next to conventional carbon steel. The increasing growth of these alloys in the structural applications is because of their small self-weight, good corrosion resistance, low maintenance, high recyclability, and aesthetic appearance [1]. However, one of the main drawbacks of aluminium alloys is their low Young's modulus, which could cause a stability issue of aluminium structural members. Moreover, the important aspects of stress-strain relationship of these alloys such as, the absence of yield plateau and continuous strain-hardening behaviour could lead to inaccurate estimation of design strength using current design codes, which are based on bi-linear stress-strain behaviour. Therefore, further research is required to evaluate the actual behaviour of aluminium structural members.

Research on axial load carrying capacity and stability response of aluminium alloy columns started in the middle of the last century. In 1938, Templin et al. [2] experimentally studied the bearing capacities of columns extruded from different aluminium alloys. Marin [3] conducted research on load-displacement curves of aluminium alloy columns under eccentric loading. From 1957 to 1971, series of

[1] Corresponding author.
E-mail address: M.Gkantou@ljmu.ac.uk

tests were conducted on non-welded and welded aluminium alloy structural members subjected to compression, bending and torsion [4–8]. In 1972, Tsuruta et al. [9] conducted tests on welded aluminium alloy columns. Total 89 hollow and 62 solid columns with rectangular section were tested under concentric and eccentric axial compression and a number of formulas were proposed to establish a relationship between compressive strength and slenderness of welded columns. Hopperstad et al. [10] studied the ultimate strengths of columns extruded from 6082-T4 and 6082-T6 alloys subjected to uniform compressive loading. In 2000, Faella et al. [11] tested a total of 80 square and rectangular columns made of 6060, 6061 and 6052 aluminium alloys under axial compression and proposed a new classification system for aluminium cross-sections. Furthermore, many researchers investigated the buckling response of aluminium columns experimentally and numerically for various extruded cross-sections, such as, square and rectangular hollow sections [12–21], circular hollow sections [20–24], I-sections [13,25,26], angle sections [16,27], channel sections [28–30], and other irregular sections [31–34]. It was shown that currently available design standards for calculating the buckling resistance of aluminium columns are generally conservative.

The present study experimentally investigated the buckling response of 13 square and rectangular 6082-T6 aluminium alloy columns under axial compression. The properties of the aluminium alloy were achieved from tensile test of coupon samples. The compressive load was employed concentrically by using a knife-edge hinge to ensure pin supports on both ends of the specimens. The structural response of the aluminium alloy columns observed from the tests is presented in terms of ultimate strengths, failure modes and load-mid-height lateral displacement relationship. Finally, a comparison was drawn between the specimen strengths recorded during compression tests and design strengths calculated using Eurocode 9 [35].

2. Experimental programme

2.1. Specimens' geometry

In this study, total 13 hollow aluminium columns were tested subjected to axial compression. All specimens were extruded and fabricated by 6082-T6 heat-treated aluminium alloy. The experimental programme comprised of four test series, including two series of hollow square section (SHS) and two series of hollow rectangular section (RHS). In the first two series, total 8 SHS specimens of two nominal section types ($D \times B$), i.e., 50.8 × 50.8 and 76.2 × 76.2 were used with different nominal thicknesses (t) varied from 1.59 to 6.35 mm. In the last two series, a total of 5 RHS specimens of two nominal section types ($D \times t$), i.e., 76.2 × 3.25 and 101.6 × 3.25 were examined, where the widths (B) were varied from 25.4 to 50.8 mm. The nominal lengths (L) of all columns were 1000 mm. Before testing, the specimen dimensions were measured using a measuring tape and a digital Vernier calliper. The columns were designated based on the cross-sectional shape and nominal dimensions. For example, the label R101.6×25.4×3.25 denotes that the shape of section of the specimen is RHS and its nominal outer depth (D), nominal outer width (B) and nominal thickness (t) are 101.6 mm, 25.4 mm and 3.25 mm, respectively. Table 1 summarises the geometric dimensions of all columns.

2.2. Material properties

The specimens' material properties were achieved from tensile test of dog-bone coupon samples. The tensile coupons were cut longitudinally from the four flat faces of the specimens. The width and gauge length a coupon were 12 mm and 100 mm, respectively, as suggested in EN ISO 6892-1 [36]. The tensile tests conducted by a 50 kN displacement-control testing machine (figure 1(a)). The strain rate of 0.2 mm/min was applied until the coupons reach to fracture. During the test, a calibrated extensometer was installed to determine the deformation of the coupons.

Table 1. Specimens' geometric dimensions.

Specimen	Depth, D (mm)	Width, B (mm)	Thickness, t (mm)	Length, L (mm)	D/B	B/t
S50.8×50.8×1.59	50.7	51.0	1.61	1000	0.99	31.78
S50.8×50.8×2.64	51.1	50.9	2.63	1000	1.00	19.34
S50.8×50.8×3.25	50.6	50.6	3.13	999	1.00	16.15
S50.8×50.8×4.76	50.6	50.6	4.67	1000	1.00	10.84
S76.2×76.2×1.63	76.3	76.3	1.54	1000	1.00	49.58
S76.2×76.2×3.25	76.4	76.4	3.23	1000	1.00	23.64
S76.2×76.2×4.76	76.2	76.1	4.76	1000	1.00	16.01
S76.2×76.2×6.35	76.3	76.3	6.28	1000	1.00	12.16
R76.2×25.4×3.25	76.4	25.4	3.34	1000	3.00	7.62
R76.2×38.1×3.25	76.2	38.2	3.27	1000	1.99	11.67
R76.2×50.8×3.25	76.1	50.7	3.18	1000	1.50	15.94
R101.6×25.4×3.25	101.8	25.4	3.22	1000	4.01	7.89
R101.6×50.8×3.25	101.8	51.4	3.42	1000	1.98	15.03

The stress-strain relationships recorded from the coupon tests were utilised to obtain the specimens' properties and calibrate the Ramberg-Osgood model (equation (1)) [37]:

$$\varepsilon = \frac{\sigma}{E} + 0.002\left(\frac{\sigma}{\sigma_{0.2}}\right)^n \tag{1}$$

where σ is the stress, ε is the strain, E denotes the Young's modulus of aluminium alloy, $\sigma_{0.2}$ is the 0.2% proof stress and n is the strain hardening exponent, which can be determined by equation (2):

$$n = \frac{ln\,2}{ln\left(\frac{\sigma_{0.2}}{\sigma_{0.1}}\right)} \tag{2}$$

where $\sigma_{0.1}$ is the 0.1% proof stress. Figure 1(b) presents the measured stress-strain curve and the curve predicted by the Ramberg-Osgood model of specimen S50.8×50.8×1.6. It is observed that the aluminium alloy exhibits rounded stress-strain relationship, which is accurately captured by the Ramberg-Osgood model. The material properties of all specimens, including, E, $\sigma_{0.1}$, $\sigma_{0.2}$, σ_u (ultimate tensile stress), n and ε_f (plastic strain at fracture) are listed in table 2.

2.3. Initial geometric imperfections

Buckling can be defined as the behaviour of a structural member, which loses its stability and suddenly bends in orthogonal direction of the loading direction. When a structural member is subjected to axial compression, the anticipated failure mode is flexural member buckling (global buckling), while local buckling occurring at the plate elements of a member can also be observed before/at failure. The stability of thin-walled compression members is affected significantly by the presence of initial geometric imperfections. Thus, the magnitude of initial imperfections of all columns were measured before the test. A linear height gauge was applied to determine the imperfection values along the centrelines of all four faces of a specimen (figure 2).

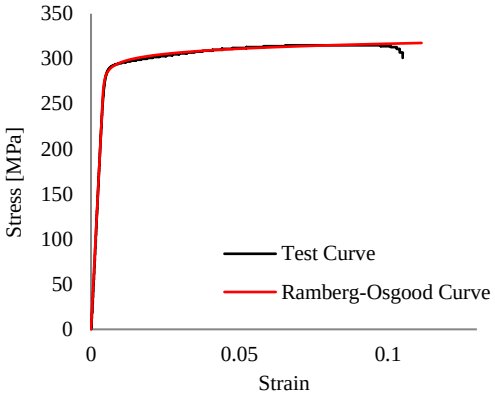

(a) (b)

Figure 1. (a) Experimental set-up of tensile coupon test, (b) comparison between measured and Ramberg-Osgood curve of specimen S50.8×50.8×1.59.

Table 2. Specimens' material properties.

Specimen	E (GPa)	$\sigma_{0.1}$ (MPa)	$\sigma_{0.2}$ (MPa)	σ_u (MPa)	n	ε_f (%)
S50.8×50.8×1.59	65.0	284.4	289.1	315	42.29	10.5
S50.8×50.8×2.64	72.2	333.9	337.1	352	72.67	9.8
S50.8×50.8×3.25	71.7	297.5	302.2	330	44.22	8.9
S50.8×50.8×4.76	67.5	302.8	305.9	325	68.05	15.5
S76.2×76.2×1.63	67.9	288.4	292.9	316	44.77	8.4
S76.2×76.2×3.25	66.2	295.2	299.1	321	52.8	10.5
S76.2×76.2×4.76	64.7	303.7	306.1	316	88.06	9.7
S76.2×76.2×6.35	69.3	290.4	295.3	326	41.43	15.3
R76.2×25.4×3.25	68.9	271.8	277.9	316	31.23	14.3
R76.2×38.1×3.25	68.5	270.4	276.8	315	29.63	9.3
R76.2×50.8×3.25	67.5	285.9	289.5	312	55.39	9.1
R101.6×25.4×3.25	63.9	234.7	242.50	290	21.20	13.2
R101.6×50.8×3.25	60.0	176.9	183.8	225	18.12	14.9

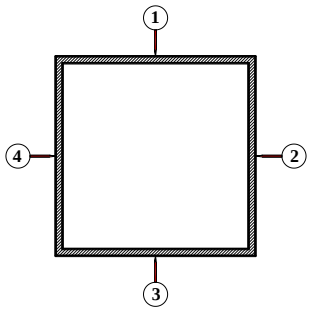

(a) (b)

Figure 2. (a) Imperfection measurement set-up, (b) location of imperfection measurements.

The local imperfection (ω_l) is defined as the maximum deformation of a column face from a flat datum. For this purpose, data were taken at regular intervals along the longitudinal direction of all faces and the maximum value measured among the four faces was taken as the local imperfection amplitude of a specimen. The initial bow (ω_g) was calculated from the deformation readings recorded at mid-length and both ends of a column. The measured results of local and global geometric imperfections are listed in table 3.

2.4. Axial compression test

A hydraulic testing machine with 600 kN capacity was used to conduct axial compression tests. Prior to the tests, top and bottom end of a specimen were milled flat for ensuring uniform distribution of applied load. Moreover, carbon fibre reinforced polymer was used to strengthen both ends of the specimens to prevent localised failure at ends. Specimens were placed accurately into the testing machine using a geometric cantering method to avoid the possibility of eccentric loading. A bearing system, consisting of a steel plate with V-shaped grooves and a knife-edge wedge was adopted at both top and bottom supports to simulate pin-ended support conditions and allow rotation of a specimen about the weak axis. Moreover, in both ends of each specimen, plates bolted to channel sections allowed the adjustment of the specimen's relative position and prevented springing out of specimens during testing, without providing any additional restraint. A displacement control load was employed at a constant rate of 0.2 mm/min excluding the presence of dynamic effects [39]. During the tests, four linear variable differential transformers (LVDTs) were used; two were positioned at the mid-height of the specimen to record lateral displacement; and two were located at the bottom channel section to monitor rotation. For measuring strain values, four strain gauges were installed symmetrically in the four outer faces at the mid-length of a specimen. A data logger was utilised to acquire the data from the strain gauges, LVDTs and load cell. The experimental setup and position of strain gauges and LVDTs are presented in figure 3.

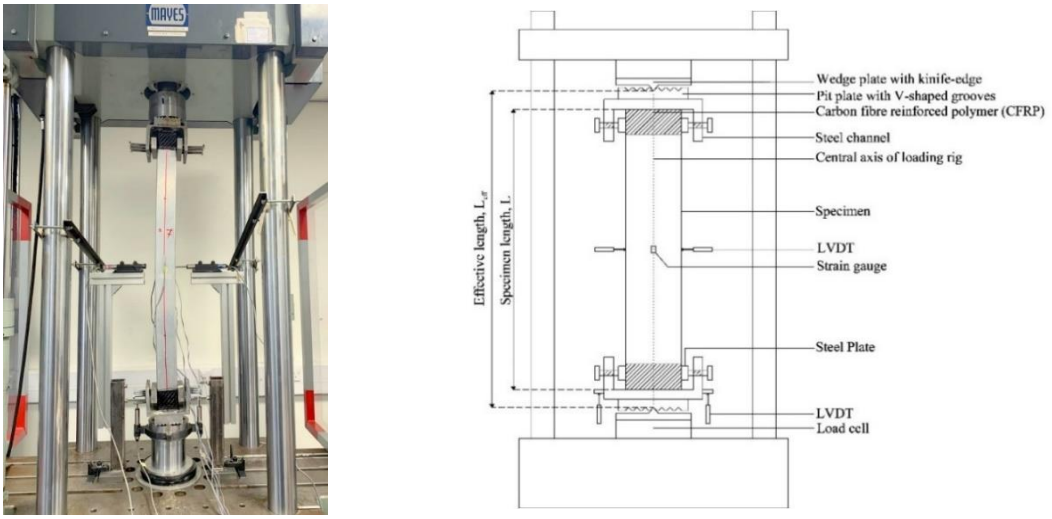

(a) (b)

Figure 3. Experimental setup and instrumentation: (a) photograph, (b) illustrative drawing.

3. Experimental investigation

3.1. Specimen geometry

In the first stages of testing, the actual initial loading eccentricity (e_0) of a specimen is calculated using the strain gauges values and the LVDTs readings (equation (3)) [38].

$$e_0 = \frac{EI\left(\varepsilon_{max} - \varepsilon_{min}\right)}{DN} - \Delta - \omega_g \tag{3}$$

In the above equation, I is the moment of inertia, N is the applied load, ε_{max}, ε_{min} are the maximum and minimum strain values corresponding to N respectively, Δ is the lateral displacement at the mid-height and D is the depth of the specimen.

3.2. Axial load-mid-height lateral displacement behaviour

During testing, the axial load-mid-height lateral displacement relationships were recorded (figure 4) and studied to understand the overall structural behaviour of all tested columns. The axial compressive load and mid-height lateral displacements were obtained from the load cell and the LVDTs respectively. All the curves show almost similar trend and can be categorised into three different regions, i.e., the elastic region, the elastic-plastic region, and the descending region. In the elastic region, the lateral displacement increases linearly and gradually with the increase of load. At the elastic-plastic region, the increase of axial load slows down to reach the peak load while the development of lateral displacement accelerates. In this region, non-linear behaviour is evident. At the last region, the lateral displacement increases rapidly together with a gradual fall of the load. As anticipated, the performance improves for B constant and increasing thickness (t) (figures 4(a) and 4(b)), and for t constant and decreasing cross-sectional aspect ratio (D/B) (figures 4(c) and 4(d)).

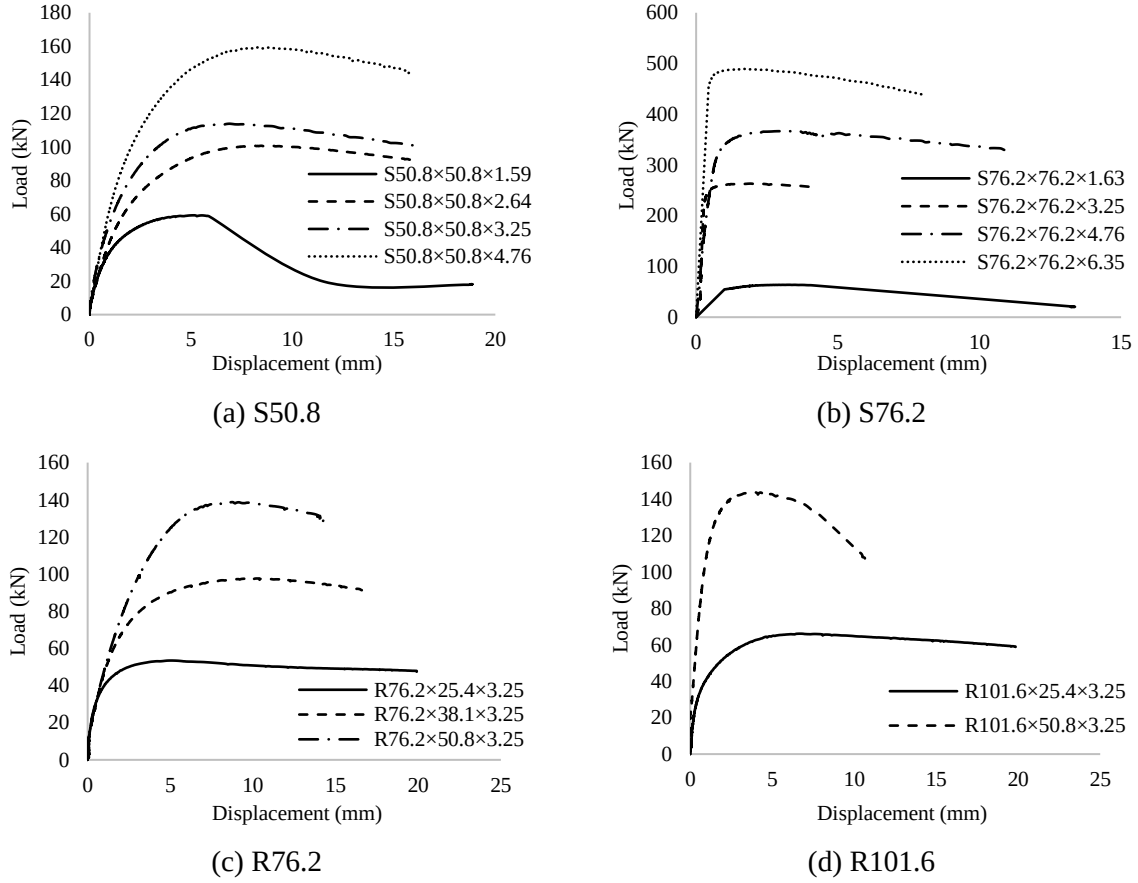

(a) S50.8 (b) S76.2

(c) R76.2 (d) R101.6

Figure 4. Load-mid-height lateral displacement relationships of specimens.

3.3. Failure mode and ultimate capacity

As the knife-edge allowed rotation about the minor axis, all specimens failed due to flexural buckling about the weak axis. No tear or cracks were identified in any specimen. In addition to global buckling, the specimens S50.8×50.8×1.59, S76.2×76.2×1.63 and S76.2×76.2×3.25, which have higher width-to-thickness (B/t) ratios also experienced local buckling near the mid-height (i.e., interactive global and local buckling). Figure 5 illustrates typical failure modes. The ultimate capacity ($N_{u,EXP}$) of a specimen is defined as the maximum applied load during the test. It is observed that in the case of square specimens the $N_{u,EXP}$ increased with the decrease of B/t ratios (B constant, t variable), whereas for rectangular sections, $N_{u,EXP}$ increased with the increase of B/t (t constant, B variable). Table 3 presents the local and global geometric imperfections, actual initial loading eccentricities, ultimate capacities, failure modes and corresponding B/t ratios of all specimens.

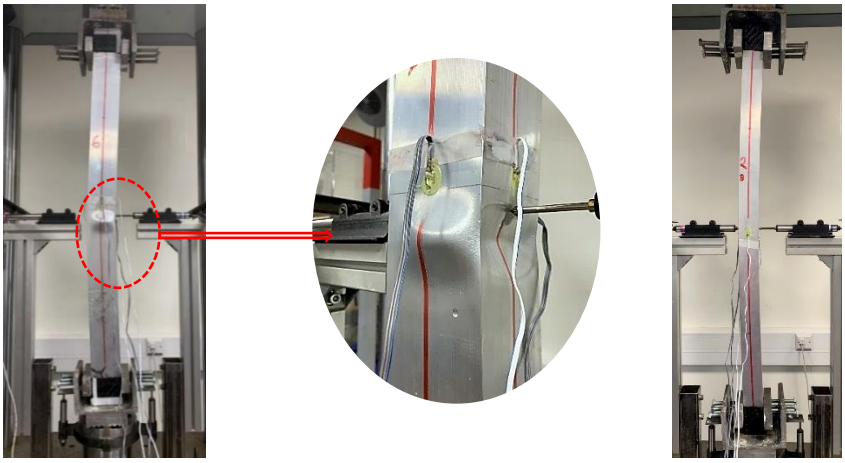

(a) (b)

Figure 5. Failure modes of (a) specimen S76.2×76.2×3.25 (Interaction of local and flexural buckling), (b) specimen S50.8×50.8×2.64 (Flexural buckling)

Table 3. Initial geometric imperfections, initial loading eccentricities, ultimate capacities and corresponding failure modes of specimens.

Specimen	ω_l (mm)	ω_g (mm)	e_o (mm)	B/t	$N_{u,EXP}$ (kN)	Failure mode
S50.8×50.8×1.59	0.11	0.03	0.45	31.78	60.22	Global with Local buckling
S50.8×50.8×2.64	0.43	0.06	1.93	19.34	100.68	Global buckling
S50.8×50.8×3.25	0.17	0.04	1.25	16.15	113.83	Global buckling
S50.8×50.8×4.76	0.19	0.01	1.83	10.84	161.48	Global buckling
S76.2×76.2×1.63	0.25	0.33	1.61	49.58	63.88	Global with Local buckling
S76.2×76.2×3.25	0.31	0.19	1.03	23.64	263.28	Global with Local buckling
S76.2×76.2×4.76	0.08	0.05	0.70	16.01	367.36	Global buckling
S76.2×76.2×6.35	0.18	0.04	0.62	12.16	489.85	Global buckling
R76.2×25.4×3.25	0.54	0.15	0.38	7.62	53.46	Global buckling
R76.2×38.1×3.25	0.06	0.02	1.12	11.67	97.62	Global buckling
R76.2×50.8×3.25	0.68	0.42	2.55	15.94	138.72	Global buckling
R101.6×25.4×3.25	0.46	0.10	1.47	7.89	66.09	Global buckling
R101.6×50.8×3.25	0.17	0.05	0.76	15.03	143.72	Global buckling

4. Comparison of experimental results with European design rules

The Eurocodes suite consists of 10 European Standards for structural design and Eurocode 9 (EN 1999-1-1) [35] provides design formulae for aluminium alloy structures. The results obtained herein are also used for the assessment of the aforementioned codified rules. According to Eurocode 9 [35] aluminium structural members subjected to axial compression could collapse by flexural or local buckling. The effective thickness method [35] is adopted to take into account the local buckling influence on the ultimate strength of specimens. The design strengths ($N_{u,EC9}$) of the specimens are estimated by the design equation given in Eurocode 9:

$$N_{u,EC9} = min(N_{c,Rd}, N_{b,Rd}) \tag{4}$$

where $N_{c,Rd}$ is the design resistance to compression and $N_{b,Rd}$ is the design resistance to buckling. $N_{c,Rd}$ is calculated by equation (5):

$$N_{c,Rd} = A_{eff} f_y / \gamma_{M1} \tag{5}$$

where A_{eff} is the effective cross-sectional area for class 4 (i.e., sections prone to local buckling) or gross cross-sectional area for class 1, 2 and 3, f_y is the proof stress and γ_{M1} is the safety coefficient. The A_{eff} can be obtained by factor down the plate thickness using a coefficient ρ_c, which is estimated by equation (6):

$$\rho_c = \frac{32}{(\beta/\varepsilon)} - \frac{220}{(\beta/\varepsilon)^2} \quad for\ \beta/\varepsilon > 22 \tag{6}$$

where β is the ratio of width-to-thickness (b/t) and $\varepsilon = \sqrt{250/f_y}$. $N_{b,Rd}$ can be determined by the equation (7):

$$N_{b,Rd} = \chi A_{eff} f_y / \gamma_{M1} \tag{7}$$

where χ is the reduction coefficient to consider the influence of flexural buckling phenomenon on the capacity of the specimens. This factor is evaluated by equation (8):

$$\chi = \frac{1}{\phi + \left(\phi^2 - \bar{\lambda}^2\right)^{0.5}} \le 1.0 \tag{8}$$

where the parameter ϕ and the relative slenderness $\bar{\lambda}$ are calculated by equations (9) and (10), respectively:

$$\phi = 0.5\left[1 + \alpha\left(\bar{\lambda} - 0.1\right) + \bar{\lambda}^2\right] \tag{9}$$

$$\bar{\lambda} = \sqrt{\frac{A_{eff} f_y}{N_{cr}}} \tag{10}$$

where α is the imperfection factor and N_{cr} is the critical elastic load which is derived by the equation (11):

$$N_{cr} = \frac{\pi^2 (EI)_{eff}}{L_{eff}^2} \tag{11}$$

where $(EI)_{eff}$ is the effective flexural rigidity and L_{eff} is the effective length of specimens.

Upon calculating the design strengths from equations (4)-(11), the main results are presented in table 4, where the buckling capacities of the aluminium alloy columns recorded during the axial compression tests ($N_{u,EXP}$) are compared with design predictions according to Eurocode 9 ($N_{u,EC9}$). The mean value and the corresponding coefficient of variation (COV) of test strength to design strength ratio are 1.36 and 0.17, respectively. In line with previous studies [18, 22, 24], it is found that the buckling capacities determined by Eurocode 9 are quite conservative.

Table 4. Comparisons of the experimental results to the design strengths of Eurocode 9.

Specimen	$\overline{\lambda}$	β/ε	Class	$N_{u,EC9}$ (kN)	$N_{u,EXP}$ (kN)	$N_{u,EXP}/N_{u,EC9}$
S50.8×50.8×1.59	1.11	31.81	4	38.35	60.22	1.57
S50.8×50.8×2.64	1.17	20.22	3	84.64	100.68	1.19
S50.8×50.8×3.25	1.13	15.57	2	93.03	113.83	1.22
S50.8×50.8×4.76	1.21	9.79	1	123.89	161.48	1.30
S76.2×76.2×1.63	0.72	51.49	4	54.69	63.88	1.17
S76.2×76.2×3.25	0.76	23.67	4	198.10	263.28	1.33
S76.2×76.2×4.76	0.80	15.52	2	295.79	367.36	1.24
S76.2×76.2×6.35	0.77	11.05	2	376.18	489.85	1.30
R76.2×25.4×3.25	2.10	22.01	4	32.60	53.46	1.64
R76.2×38.1×3.26	1.39	22.38	4	74.37	97.62	1.31
R76.2×50.8×3.25	1.08	23.58	4	116.88	138.72	1.19
R101.6×25.4×3.25	1.96	29.18	4	33.60	66.09	1.97
R101.6×50.8×3.25	0.88	23.81	4	117.78	143.72	1.22
			Average			1.36
			COV			0.17

5. Conclusions

The present study experimentally investigated the buckling response of 13 square and rectangular 6082-T6 aluminium alloy columns under axial compression. The specimens' initial geometric imperfections were measured before the tests. The aluminium alloy properties were determined by tensile test of dog-bone coupon samples. The structural response of all specimens obtained from the compression tests was reported in terms of ultimate loads, load-mid-height lateral displacement and failure modes. It is observed that all tested columns were failed by overall flexural buckling, whereas three of them with large width-to-thickness ratios (B/t) were experienced failure due to local-global interactive buckling. A comparison was drawn between the specimen strengths recorded during compression tests and design strengths predicted using Eurocode 9. The comparison showed that the design formulae provided by Eurocode 9 are conservative, i.e., mean of $N_{u,EXP}/N_{u,EC9}$ equal to 1.36 and COV equal to 0.17. Further investigation for the provision of more accurate formulae is recommended.

Acknowledgments

The authors are grateful to the technicians of Civil Engineering and Mechanical Engineering Departments of Liverpool John Moores University for their valuable assistance. In addition, the financial support of the Faculty of Engineering and Technology of Liverpool John Moores University is gratefully acknowledged.

References

[1] Georgantzia E, Gkantou M and Kamaris GS 2021 Aluminium alloys as structural material: A

review of research *Eng. Struct.* **227** 111372
[2] Templin RL, Strum RG, Hartman EC and Holt M 1938 *Column strength of various aluminum alloys* (Pittsburgh: Aluminum Company of America) Technical paper No. 1
[3] Marin J 1947 Creep deflections in columns *J. Appl. Phys.* **18** 103–9
[4] Clark JR and Jombock JW 1957 Lateral buckling of I-beams subjected to unequal end moments *J. Eng. Mech. Div. ASCE* **83** 1–19
[5] Brungraber RJ and Clark JW 1962 Strength of welded aluminum columns *J. Struct. Div, ASCE* **127** 202–26
[6] Hill HN and Clark JW 1960 Brungraber RJ. Design of welded aluminum structures *J. Struct. Div. ASCE* **86** 101–24
[7] Clark JW and Rolf RL 1964 Design of aluminum tubular members *J. Struct. Div. ASCE* **90** 259–89.
[8] Clark JW 1971 *Formulas for Design of Welded Columns* (Pittsburgh: Aluminum Company of America) Report No. 12-71-23
[9] Tsuruta A, Sakurai J and Horikawa K 1972 Buckling strength of welded aluminium columns *Trans. Japan Weld. Soc.* **3** 285–91
[10] Hopperstad OS, Langseth M and Tryland T 1999 Ultimate strength of aluminium alloy outstands in compression: experiments and simplified analysis *Thin-Walled Struct.* **34** 279–94
[11] Faella C, Mazzolani FM, Piluso V and Rizzano G 2000 Local buckling of aluminium members: testing and classification *J. Struct. Eng.* **126** 353–60
[12] Zhu JH and Young B 2006 Tests and design of aluminum alloy compression members *J. Struct. Eng.* **132** 1096–1107
[13] Zhai XM, Wang YJ, Wu H and Fan F 2011 Research on stability of high strength aluminum alloy columns loaded by axial compressive load *Adv. Mater. Res.***168** 1915–20
[14] Su MN, Young B and Gardner L 2014 Testing and design of aluminum alloy cross sections in compression *J. Struct. Eng. ASCE* **140**(9) 04014047
[15] Georgantzia E, Gkantou M, Kamaris GS, Kansara K and Hashim K 2020 Aluminium alloy cross-sections under uniaxial bending and compression: A numerical study *Proc. of In IOP Conference Series: Materials Science and Engineering. IOP Publishing.* (Accepted)
[16] Ali SB, Kamaris GS, Gkantou M, Kansara K and Hashim K 2020 Numerical study of concrete-filled aluminium alloy tubular columns under eccentric compression *Proc. of In IOP Conference Series: Materials Science and Engineering. IOP Publishing.* (Accepted)
[17] Feng R, Zhu W, Wan H, Chen A and Chen Y 2018 Tests of perforated aluminium alloy SHSs and RHSs under axial compression *Thin-Walled Struct.* **130** 194–212
[18] Wang ZX, Wang YQ, Sojeong J and Ouyang YW 2018 Experimental investigation and parametric analysis on overall buckling behavior of large-section aluminum alloy columns under axial compression *Thin-Walled Struct. 122* 585–96
[19] Feng R and Liu J 2019 Numerical investigation and design of perforated aluminium alloy SHS and RHS columns *Eng. Struct.* **199** 109591
[20] Zhao Y, Zhai X and Wang J 2019 Buckling behaviors and ultimate strengths of 6082-T6 aluminum alloy columns under eccentric compression – Part I: Experiments and finite element modelling *Thin-Walled Struct.* **143** 106207
[21] Zhao Y, Zhai X and Wang J 2019 Buckling behaviors and ultimate strength of 6082-T6 aluminum alloy columns with square and circular hollow sections under eccentric compression – Part II: Parametric study, design provisions and reliability analysis *Thin-Walled Struct.* **143** 106208
[22] Zhu JH and Young B 2006 Experimental investigation of aluminum alloy circular hollow section columns *Eng. Struct.* **28** 207–15
[23] Feng R, Mou X, Chen A and Ma Y 2016 Tests of aluminium alloy CHS columns with circular openings *Thin-Walled Struct.* **109** 113–31
[24] Wang YJ, Fan F and Lin SB 2015 Experimental investigation on the stability of aluminum alloy 6082 circular tubes in axial compression *Thin-Walled Struct.* **89** 54–66
[25] Adeoti GO, Fan F, Wang YJ and Zhai XM 2015 Stability of 6082-T6 aluminum alloy columns with H-section and rectangular hollow sections *Thin-Walled Struct.* **89** 1–16

[26] Bock M, Gkantou M, Theofanous M 2019 Slenderness limits of aluminium outstand elements subjected to stress gradients *Proc. of 9th International Conference on Steel and aluminium structures* (Bradford, UK)
[27] Wang YQ, Wang ZX, Hu XG, Han JK and Xing HJ 2016 Experimental study and parametric analysis on the stability behavior of 7A04 high-strength aluminum alloy angle columns under axial compression *Thin-Walled Struct.* **108** 305–20
[28] Huynh LAT, Pham CH and Rasmussen KJR 2016 Stub Column Tests and Finite Element Modelling of Cold-Rolled Aluminium Alloy 5052 Channel Sections *Proc. Eighth Int. Conf. STEEL Aluminium Structures* (December 7 – 9 Hong Kong)
[29] Zhu JH, Li ZQ, Su MN and Young B 2019 Behaviour of aluminium alloy plain and lipped channel columns *Thin-Walled Struct.* **135** 306–16
[30] Zhu JH, Li ZQ, Su MN and Young B 2019 Numerical study and design of aluminium alloy channel section columns with welds *Thin-Walled Struct.* 139–50
[31] Liu M, Zhang L, Wang P and Chang Y 2015 Experimental investigation on local buckling behaviors of stiffened closed-section thin-walled aluminum alloy columns under compression *Thin-Walled Struct.* **94** 188–98
[32] Liu M, Zhang L, Wang P and Chang Y 2015 Buckling behaviors of irregular section aluminum alloy columns under axial compression *Eng. Struct.* **95** 127–37
[33] Chang Y, Liu M and Wang P 2016 Interacted buckling failure of thin-walled irregular-shaped aluminum alloy column under axial compression *Thin-Walled Struct.* **107** 627–47
[34] Chang Y, Liu M, Wang P and Li X 2017 Behaviors and design method for distortional buckling of thin-walled irregular-shaped aluminum alloy struts under axial compression *Eng. Struct.* **153** 118–35
[35] EN 1999-1-1 2007 *Eurocode 9: Design of aluminium structures. Part 1-1: General structural rules - General structural rules and rules for buildings* (Brussels: European Committee for Standardization)
[36] EN ISO 6892-1 2009 *Metallic Materials – Tensile Testing – Part 1: Method of Test at Room Temperature* (Brussels: European Committee for Standardization)
[37] Ramberg W and Osgood WR 1943 *Description of stress-strain curves by three parameters* (Washington: National advisory committee for aeronautics) Technical Note No. 902
[38] Gkantou M, Theofanous M, Wang J, Baniotopoulos C and Gardner L 2017 Behaviour and design of high strength steel cross-sections under combined loading *Proc. of the Inst. of Civil Engineers-Structures and Buildings* (United Kingdom)
[39] Wang J, Afshan S, Gkantou M, Theofanous M, Baniotopoulos C and Gardner L 2016 Flexural behaviour of hot-finished high strength steel square and rectangular hollow sections *J Constr. Steel. Res.* **121** 97-109